Check for updates

ORIGINAL ARTICLE

Prenatal VEGF Nanodelivery Reverses Congenital Diaphragmatic Hernia–associated Pulmonary Abnormalities

Stavros P. Loukogeorgakis[1,6,7*], Federica Michielin[1*], Noura Al-Juffali[4*], Julio Jimenez[7,9*], Soichi Shibuya[1*], Jessica Allen-Hyttinen[4*], Mary Patrice Eastwood[7*], Ahmed S. N. Alhendi[4], Joseph Davidson[1], Eleonora Naldi[1], Panagiotis Maghsoudlou[1], Alfonso Tedeschi[1], Sahira Khalaf[1], Manuela Platé[4], Camila Fachin[6,11,12], Andre Dos Santos Dias[6,11,12], Nikhil Sindhwani[7], Dominic Scaglioni[1], Theodoros Xenakis[2], Neil Sebire[3], Monica Giomo[13], Simon Eaton[1,5], Jaan Toelen[7,10], Camilla Luni[14], Piero Pavan[13,15], Peter Carmeliet[8,16], Francesca Russo[7,10], Samuel Janes[4], Marko Z. Nikolić[4*], Nicola Elvassore[1*], Jan Deprest[5,7,10*], and Paolo De Coppi[1,7,17*]

[1]Stem Cells and Regenerative Medicine, [2]Genetics and Genomic Medicine, and [3]Population, Policy and Practice, Great Ormond Street Institute of Child Health, [4]UCL Respiratory, Division of Medicine, and [5]Research Department of Maternal Fetal Medicine, UCL Institute for Women's Health, University College London, London, United Kingdom; [6]Center for Fetal Research, The Children's Hospital of Philadelphia, Philadelphia, Pennsylvania; [7]Department of Development and Regeneration, Woman and Child, Group Biomedical Sciences, and [8]Laboratory of Angiogenesis and Vascular Metabolism, Department of Oncology, KU Leuven, Leuven, Belgium; [9]Department of Obstetrics and Gynecology, Clinica Alemana Santiago, Universidad del Desarrollo, Santiago, Chile; [10]Department of Obstetrics and Gynecology, Division of Woman and Child, University Hospitals Leuven, Leuven, Belgium; [11]Division of Pediatric Surgery, Federal University of São Paulo, Sao Paulo, Brazil; [12]Division of Pediatric Surgery, Federal University of Paraná, Curitiba, Brazil; [13]Department of Industrial Engineering, University of Padova, Padova, Italy; [14]Department of Civil, Chemical, Environmental and Materials Engineering, University of Bologna, Bologna, Italy; [15]Fondazione Istituto di Ricerca Pediatrica Città della Speranza, Padova, Italy; [16]Laboratory of Angiogenesis and Vascular Metabolism, Vesalius Research Center, VIB, Leuven, Belgium; and [17]Department of Surgery, Great Ormond Street Hospital for Children National Health Service Foundation Trust, London, United Kingdom

ORCID IDs: 0000-0002-2960-5252 (S.P.L.); 0000-0003-2065-6851 (F.M.); 0000-0002-1659-0207 (P.D.C.).

Downloaded from academic.oup.com/ajrccm/article/211/6/992/8513773 by Universidad de Desarrollo user on 16 November 2026

Abstract

Rationale: Congenital diaphragmatic hernia (CDH) results in lung hypoplasia. In severe cases, tracheal occlusion (TO) can be offered to promote lung growth. However, the benefit is limited, and novel treatments are required to supplement TO. VEGF (vascular endothelial growth factor) is downregulated in animal models of CDH and could be a therapeutic target, but its role in human CDH is not known.

Objectives: To investigate whether VEGF supplementation could be a suitable treatment for CDH-associated lung pathology.

Methods: Fetal lungs from patients with CDH were used to determine pulmonary morphology and VEGF expression. A novel human *ex vivo* model of fetal lung compression recapitulating CDH features was developed and used to determine the effect of exogenous VEGF supplementation. A nanoparticle-based approach for intrapulmonary delivery of VEGF was developed by conjugating it on functionalized nanodiamonds, which was tested in experimental CDH *in vivo*.

Measurements and Main Results: VEGF expression was downregulated in the distal pulmonary epithelium of human CDH fetuses in conjunction with attenuated cell proliferation. The compression model resulted in impaired branching morphogenesis similar to CDH and downregulation of VEGF expression in conjunction with reduced proliferation of terminal bud epithelial progenitors; these could be reversed by exogenous supplementation of VEGF. Prenatal delivery of VEGF with the functionalized nanodiamond VEGF platform in CDH fetal rats resulted in lung growth and pulmonary arterial remodeling that was complementary to that achieved by TO alone with appearances comparable to healthy controls.

Conclusions: This innovative approach could have a significant impact on the treatment of CDH.

Keywords: congenital diaphragmatic hernia; VEGF; nanoparticles; mechanical compression; alveolar epithelium

(Received in original form February 8, 2024; accepted in final form February 13, 2025)

*These authors contributed equally to this work.

Am J Respir Crit Care Med Vol 211, Iss 6, pp 992–1006, Jun 2025
Copyright © 2025 by the American Thoracic Society
Originally Published in Press as DOI: 10.1164/rccm.202401-0161OC on February 18, 2025
Internet address: www.atsjournals.org

Pulmonary hypoplasia is a major cause of neonatal mortality (rates of 70–95% perinatally) (1). Congenital diaphragmatic hernia (CDH) is one of the major causes; it is characterized by herniation of abdominal viscera into the thorax, resulting in impaired lung development, reduced airway branching/alveolar surface area, and pulmonary hypertension (2, 3). Severe/extreme CDH is associated with mortality rates >75% (4) and can be diagnosed antenatally, enabling prenatal therapy. Currently, tracheal occlusion (TO), involving percutaneous balloon insertion into the fetal trachea (5, 6), is the only *in utero* intervention available to fetuses with compromised lung development (7). Even with TO, mortality rates remain around 50% (8), necessitating novel therapies to complement TO (9).

CDH animal models have shown impairment of the VEGF (vascular endothelial growth factor) pathway. VEGF levels are reduced in hypoplastic lungs from rats with nitrofen-induced CDH (10–13), and prenatal pharmacological disruption of VEGF signaling resulted in hypoplasia and pulmonary hypertension in rodents and sheep (14–16). Moreover, VEGF administration *in vitro* accelerated growth in nitrofen-induced hypoplastic rat lung explants (17) and normalized function of pulmonary artery endothelial cells derived from fetal lambs with CDH (18). Nevertheless, the role of VEGF in human CDH is not known. A major contributor to the CDH pulmonary phenotype is mechanical compression of herniated organs into the chest cavity. However, in the nitrofen model, lung maldevelopment occurs earlier than herniation (9), so teratogenic versus mechanical effects are difficult to distinguish, whereas surgical models of CDH are limited to late stages of development, which do not accurately recapitulate the disease (19).

Although the benefits of VEGF administration have been demonstrated in models of prematurity-associated respiratory distress syndrome (20, 21), it is not known whether VEGF administration has an effect on CDH. Successful use of exogenous VEGF in this context would necessitate a delivery method allowing VEGF release in a sustained and targeted manner. The latter is particularly important because of the rapid plasma clearance of VEGF, as well as its key role in tumor growth (22). Nanoparticle-based delivery platforms are currently being investigated in various fields of medicine (23–25) and may also have significant translational potential in the setting of CDH-associated pulmonary pathology. Nanodiamonds (NDs) are one such platform that allows the conjugation and sustained release of a broad range of therapeutic agents (25, 26).

Some of the results of these studies have been previously reported in the form of a preprint (*bioRxiv*, 23 Feb 2024, https://doi.org/10.1101/2024.02.20.581170).

Methods

Mouse and Human Fetal Lung Tissue for *In Vitro* Study

Whole lungs from gestational day 12.5 (E12.5) mouse embryos were obtained as previously reported (27). Whole fetal lung samples aged 7–8 postconception weeks were obtained under permission from the National Health Service Research Ethical Committee

Supported by a Wellcome Trust postdoctoral fellowship for M.B./Ph.D. graduates (ref. no. 098539/Z/12/Z to S.P.L.), a National Institute for Health and Care Research Biomedical Research Centres Catalyst Fellowship (F.M.), Rosetrees Trust grant Seedcorn2020/100052 (F.M.), BREATH Consortium for Lung Regeneration Longfonds (P.D.C. and F.M.), Japan Society for the Promotion of Science overseas research fellowship 310072 (S.S.), the European Commission via its Erasmus Joint Doctoral program (Erasmus+ grant 2013-0040 to J.J. and M.P.E.), the National Institute for Health Research and Wellcome Trust/Engineering and Physical Sciences Research Council "Guided Instrumentation for Fetal Therapy and Surgery" programme (P.D.C.), the Flanders Research Foundation (FWO Vlaanderen) grant 8012.07 (J.D.), the Great Ormond Street Hospital Children's Charity, Universitaire Ziekenhuizen Leuven, KU Leuven grant C32/17/054, Congenital Diaphragmatic Hernia UK, Wellcome Trust grant WT101957, Engineering and Physical Sciences Research Council grant NS/A000027/1, Medical Research Council (MRC) Clinician Scientist Fellowship MR/W00111X/1 (M.Z.N.), Rosetrees Trust grant M899 (M.Z.N.), a Rutherford Fund Fellowship allocated by the MRC UK Regenerative Medicine Platform 2 (MR/5005579/1; M.Z.N.), and the University College London Birkbeck MRC Doctoral Training Programme (J.A-H.). This publication represents the views of the authors, and the European Commission cannot be held responsible for any use that may be made from the information contained herein.

Patent details: "Means and Methods for Treating Lung Hypoplasia" (Inventors: S.P.L., N.A-J., P.C., J.D., P.D.C.; Publication Number: WO 216/198121 A1; Publication Date: 15/12/2016).

Author Contributions: S.P.L. and F.M.: conception and design, financial support, provision of study material, collection of data, data analysis/interpretation, manuscript writing, final approval of manuscript. N.A.-J., J.J., and S.S: conception and design, collection of data, data analysis/interpretation, manuscript writing, final approval of manuscript. J.A-H: collection of data, data analysis/interpretation, manuscript writing, final approval of manuscript. M.P.E. and A.S.N.A: data collection, data analysis/interpretation, final approval of manuscript. J.D.: manuscript writing, final approval of manuscript. E.N. and P.M.: collection of data, data analysis/interpretation, final approval of manuscript. A.T. and S.K.: data analysis/interpretation, manuscript writing, final approval of manuscript. M.P.: provision of study material, final approval of manuscript. C.F.: data analysis/interpretation, manuscript writing, final approval of manuscript. A.D.S.D.: data analysis/interpretation, manuscript writing, final approval of manuscript. N. Sindhwani, D.S., and T.X.: collection of data, final approval of manuscript. N. Sebire: provision of study material, final approval of manuscript. M.G.: analysis/interpretation, final approval of manuscript. S.E.: data analysis/interpretation, final approval of manuscript. J.T.: data analysis/interpretation, manuscript writing, final approval of manuscript. C.L.: data analysis/interpretation, final approval of manuscript. P.P.: data analysis/interpretation, manuscript writing, final approval of manuscript. P.C.: financial support, provision of study material, data analysis/interpretation, manuscript writing, final approval of manuscript. F.R.: data analysis/interpretation, final approval of manuscript. S.J.: financial support, provision of study material, data analysis/interpretation, manuscript writing, final approval of manuscript. M.Z.N. and N.E.: conception and design, financial support, provision of study material, data analysis/interpretation, manuscript writing, final approval of manuscript. J.D.: conception and design, financial support, provision of study material, data analysis/interpretation, manuscript writing, final approval of manuscript. P.D.C.: conception and design, financial support, provision of study material, data analysis/interpretation, manuscript writing, final approval of manuscript.

Correspondence and requests for reprints should be addressed to Paolo De Coppi, M.D., Ph.D., Developmental Biology and Cancer Programme, UCL Great Ormond Street Institute of Child Health, 30 Guilford Street, London WC1N 1EH, UK. E-mail: p.decoppi@ucl.ac.uk.

This article has a related editorial.

A data supplement for this article is available via the Supplements tab at the top of the online article.

Artificial Intelligence Disclaimer: No artificial intelligence tools were used in writing this manuscript.

Downloaded from academic.oup.com/ajrcm/article/211/6/992/8513773 by Universidad de Desarrollo user on 16 November 2026

At a Glance Commentary

Scientific Knowledge on the Subject: Congenital diaphragmatic hernia (CDH) is a fetal congenital malformation characterized by herniation of abdominal viscera into the thorax, resulting in lung compression and impaired development. Tracheal occlusion, involving percutaneous balloon insertion into the fetal trachea, represents the only *in utero* intervention available to fetuses with compromised lungs, yet it is effective in only 50% of cases. VEGF (vascular endothelial growth factor) is downregulated in animal models of CDH and could be a therapeutic target, but its role in human CDH is not known.

What This Study Adds to the Field: Our study demonstrated that VEGF expression is downregulated in the distal pulmonary epithelium of human CDH fetuses in conjunction with attenuated cell proliferation, as also confirmed in a human *ex vivo* model of fetal lung compression. This resulted in impaired branching morphogenesis similar to CDH and downregulation of VEGF expression along with reduced proliferation of terminal bud epithelial progenitors. This phenotype could be reversed by exogenous supplementation of VEGF. In addition, sustained release of nanoparticles functionalized with exogenous VEGF resulted in normalized lung size and airway morphology and improved parenchymal vascularization in two different CDH animal models, with potential scalability for clinical use.

(reference 18/LO/0822 and 18/NE/0290) and the Joint Medical Research Council/Wellcome Trust Human Developmental Biology Resource (www.hdbr.org). *See* online supplement for information on the ancestral background of the tissue.

Three-Dimensional Printing

For three-dimensional (3D) printing, 10 μl of 20% 7-hydroxycoumarin-3-carboxylate - polyethylene glycol conjugated gel (PEG-HCC) in PBS solution was added on Matrigel-embedded lung samples. The 3D printing was performed as previously reported (28). Confocal microscope settings for cross-linking were as follows: pixel resolution, 1,640 × 1,640; pixel dwell time, 0.98 μs, zoom, ×0.9; laser wavelength, 800 nm; stack depth, 2 μm; laser power, 80%; and 4× immersion objective. Control samples were incubated with the same amount of PEG-HCC gel but without cross-linking.

Production of ND-VEGF Conjugates

Powder detonation ND hydrogels (2–8 nm) were purchased from the Nanocarbon Research Institute (NanoAmando). VEGF conjugation on NDs was performed using a sequential process described in the online supplement and in the Results section. Briefly, NDs with a primary amine group (ND-NH_2) were coupled to a sulfhydryl-to-amine cross-linker, Sulfo-LC-SPDP (sulfosuccinimidyl 6-[3′-(2-pyridyldithio)-propionamido] hexanoate). The amine-reactive NHS ester arm of the linker reacted with ND-NH_2 to form a stable amide bond (ND-SPDP) while the pyridyldithiol arm reacted with thiol-modified (thiolated) VEGF to yield reducible disulfide bonds (29–31) (Figure E7A in the online supplement).

Animals for *In Vivo* Study

All experimental protocols were approved by the Ethics Committee for Animal Experimentation of the Faculty of Medicine of KU Leuven (rat, P102/2015; rabbit, P171/2013) and follow the ARRIVE 2.0 reporting guidelines. Gestational day (E) 19–21 fetuses from time-dated pregnant Wistar rats and E23–E30 fetuses from time-dated pregnant rabbits (New Zealand White/Dendermonde) were used.

Generation of CDH

To generate fetuses with CDH and hypoplasia, pregnant rats received 100 mg of nitrofen on E9 as previously described (11, 12, 32). In rabbit studies, surgical creation of left-sided CDH was performed at E23 (33).

Sample Size Calculation and Statistical Analysis

For rat *in vivo* experiments, sample size calculation was done based on previous studies in which TO improved several outcomes by 40% in CDH fetuses (34, 35). We expected an additional effect of 60% over the effect of TO, and thus an outcome within the range of healthy fetuses. Using as variables eight groups, α of 0.05, and β of 0.11, we calculated a minimum of eight animals per group. For rabbit *in vivo* studies, we determined that a sample size of six fetuses per group would detect a 40% reduction in medial thickness (MT) and a 40% increase in pulmonary artery acceleration/ejection time with an α of 0.05 and a β of 0.2 (36). Animals were randomized to experimental groups using an online randomization tool. For all *in vivo* experiments, team members performing surgical/intervention procedures and outcome assessments/analyses were blinded to experimental group allocation.

Data were assessed for normality using the Kolmogorov-Smirnov test. Results are expressed as mean ± standard deviation or median (range) for normally and nonnormally distributed data, respectively. For the results in Figures 1–3, groups were compared using an unpaired *t* test or Mann-Whitney test. Normal distribution was assessed via Kolmogorov-Smirnov test. For the results in Figures 4–6, one-way ANOVA with Bonferroni *post hoc* tests or the Kruskal-Wallis test with Dunn's *post hoc* tests was used. $P < 0.05$ was considered statistically significant. All analyses were performed with GraphPad Prism 7.0. *See* online supplement for descriptions of bulk and single-cell RNA sequencing (scRNA-seq) analyses.

Results

Lung Hypoplasia in Human CDH Fetal Lungs Is Associated with Reduced VEGF Expression and Epithelial Proliferation

Despite a limited number of available donors, we found noticeable hypoplasia as early as 18 weeks postconception in postmortem human CDH tissue compared with healthy lungs at matching developmental stages (Figures 1A–1C) (37). We also found significant downregulation of VEGF and VEGF receptor 2 (KDR/Flk1; $P < 0.0001$) in the distal epithelium compared with healthy controls, with an associated reduction in proliferation ($P < 0.0001$) (Figures 1D–1G). Overall, these data confirm previous findings in the nitrofen model (10). Conversely, we did not find significant differences in endothelial proliferation, the main target cell of VEGF ligands (Figure E1). We therefore hypothesized that the exogenous supplementation of VEGF to the developing lung could promote distal epithelial

Downloaded from academic.oup.com/ajrccm/article/211/6/992/8513773 by Universidad de Desarrollo user on 16 November 2026

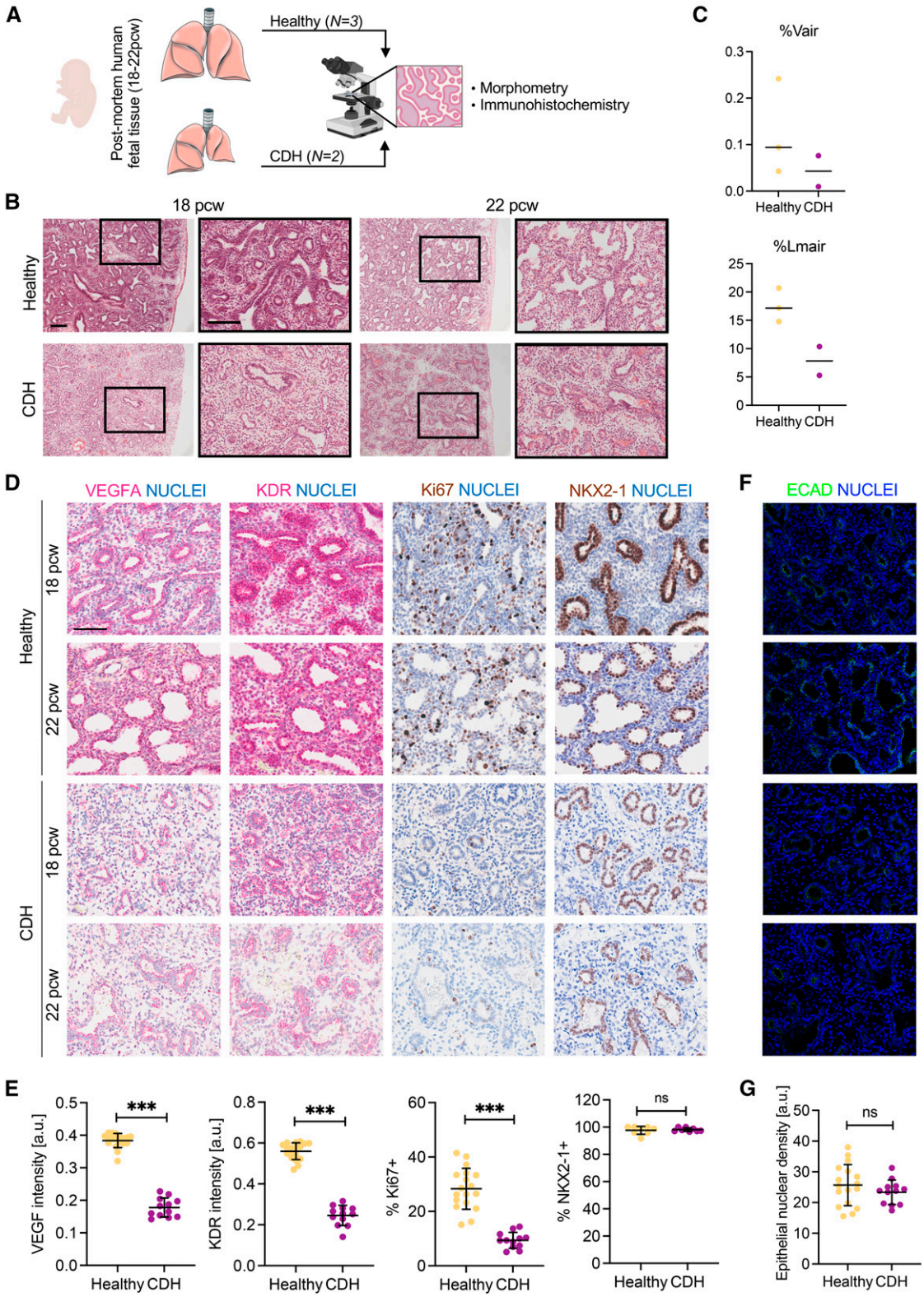


Figure 1. (*A*) Schematic illustration of the study design based on the analysis of the early-stage congenital diaphragmatic hernia (CDH) fetal lung sections to assess early hypoplasia and VEGF (vascular endothelial growth factor) impairment. (*B*) Hematoxylin and eosin staining analysis of postmortem CDH human lung tissue reveals impaired epithelial development compared with control healthy tissue at matching developmental stages. Scale bars, 100 μm. (*C*) Morphometric analysis of CDH and healthy lung tissue at 18–22 postconception weeks reveals decreased values of volume densities of air space in CDH tissues compared with healthy tissue at the same developmental stages. A similar trend can be

Downloaded from academic.oup.com/ajrccm/article/211/6/992/8513773 by Universidad de Desarrollo user on 16 November 2026

proliferation and attenuate lung hypoplasia in CDH fetuses.

Development of a Human Model of Fetal Lung Mechanical Compression Relevant to CDH

To test this hypothesis, we sought to develop an *ex vivo* model that recapitulates the mechanically constricted environment of the human fetal lung at the earliest stages of CDH. We first exposed embryonic mouse lungs to physical constraints created through hydrogels (i.e., PEG-HCC) with well-defined elastic modulus by leveraging an intravital bioprinting approach (38) that enables accurate control over the PEG-HCC cross-linking around the lung with predetermined mechanical properties (Figure 2A). Atomic force microscopy analysis confirmed the increase in stiffness of the cross-linked PEG-HCC hydrogel compared with Matrigel (Figure 2B). No cytotoxic effects as a direct consequence of the cross-linking have been observed (28, 38). The formation of a mechanically printed barrier successfully confined the growth of mouse lung tissue compared with noncompressed controls, with impairment in branching morphogenesis (Figure 2C and *see* online supplement). In addition, hematoxylin and eosin staining revealed morphological alterations of the compressed lungs with noticeable reduced airway space (Figures 2D and 2E). Pulmonary epithelial proliferation analysis demonstrated that the fraction of E-cadherin/EdU (5-ethynyl-2-deoxyuridine) double-positive cells in compressed lungs was reduced (Figure 2F). In addition, bulk RNA-seq analysis demonstrated altered transcriptional activity in the compressed lungs compared with controls, including *Vegfa* downregulation (Figures 2G and E2). Differentially expressed gene network analysis showed enrichment of Gene Ontology Biological Process categories related to inflammatory and immune responses (39, 40) (Figure 2H and *see* online supplement). To better understand how the compressed lung is subjected to mechanical load because of the confinement, we developed an *in silico* analysis based on the finite element method (FEM). We assumed a distinct proliferation rate between distal and proximal areas of the tissue that was validated by the experimental observations of surface growth (Figures E3A–E3C). Hydrostatic stress maps showed an overall increase of the mechanical load in the compressed lung with a noticeable difference between proximal and distal areas, suggesting that the bud tips are the most subjected to compression (*see* Figure E3D).

We then translated the developed *ex vivo* CDH model for human tissue investigation by using early pseudoglandular-stage human fetal lung fragments (*see* online supplement). We first verified tissue growth and viability and observed branching morphogenesis and spontaneous peristalsis for as long as 2 weeks in culture (Video E2). To mimic mechanical compression, we used PEG-HCC to 3D-print a mechanical barrier (Figure 3A). At Day 7, we observed a significant reduction in the surface area of compressed lung fragments ($P < 0.001$), as well as reduced branching morphogenesis ($P < 0.05$) (Figures 3B and 3C). FEM analysis adapted to the human model (*see* Figures E3E and E3F) showed a good representation of experimental data assuming a Young's modulus between 1 and 1.5 kPa (Figure 3D). Hydrostatic stress maps confirmed an approximate threefold increase of the mechanical load in the compressed tissue compared with control (Figure 3E). Overall, these data suggest that the mechanical confinement at an early stage is sufficient to mimic some key features of CDH pathogenesis, mainly affecting distal epithelial proliferation.

VEGF Expression and Cell Proliferation Are Impaired in Compressed Human Fetal Lung Bud Tip Progenitor Cells and Can Be Rescued by VEGF Supplementation

To further investigate the effects of mechanical compression on the human fetal lung bud tip cells, we conducted a scRNA-seq analysis of compressed and control lung fragments from three donors. We captured and identified more than 30,000 cells across 3 biological replicates, including all expected cell types with no significant differences between groups (41) (Figures 3F and E4A–E4D). Cluster annotation was performed as reported in the online supplement. Within the epithelial compartment, we identified distal epithelial cells (composed of tip, stalk, and airway progenitors), as well as neuroendocrine and very few peripheral nervous system cells. We also found a sizeable, not previously described, cluster of undifferentiated cells adjacent to the distal epithelium strongly expressing stretch-associated genes (42, 43) in addition to distal epithelial markers, but not associated with the presence of the mechanical constraint. We identified these as "stretched" epithelial cells and attributed their presence to *ex vivo* culture artifacts, as swelling of distal tips in culture was occasionally observed (Figure E5). We focused our investigation on the *SOX9*/*TESC* double-positive tip cells (41). Gene Ontology Biological Process analysis revealed several pathways significantly upregulated in compressed tips (Figures 3G and 3H); many of these signals are lost when looking at the epithelial compartment as a whole (*see* Figures E4E and E4F), indicating a heightened effect of compression on tip cells. Furthermore, we saw a reduction in known proliferation signatures (44) and VEGF-family genes in the presence of mechanical stimuli (Figure 3I).

We leveraged the human model to extend our scRNA-seq observations and test whether VEGF supplementation at concentrations based on previous murine studies (17) (Figure E6) could enhance distal epithelial proliferation (Figure 3J). Although compression impaired proliferation ($P < 0.001$), VEGF supplementation rescued it to levels similar to control lungs, but the

Figure 1. (*Continued*). observed for the mean linear intercept of air space. (*D*) Histologic analysis of VEGFA, KDR, Ki67, and NKX2-1 markers in normal ($n = 3$ donors) and CDH ($n = 2$ donors) fetal lung tissue in the range of 18–22 postconception weeks. Scale bars, 50 μm. (*E*) Quantification of epithelial VEGFA and KDR expression reported in *D* shows a significant decrease for both markers in CDH compared with healthy samples. Correspondingly, the percentage of Ki67-positive epithelial cells is significantly lower in CDH compared with healthy samples, with no significant differences in the number of NKX2-1–positive cells (unpaired *t* test, $^{***}P < 0.001$). (*F*) Immunofluorescence analysis of E-cadherin in normal and CDH fetal lung tissue. Scale bars, 100 μm. (*G*) Quantification of epithelial nuclear density based on the results in *E* shows no significant differences between CDH and healthy tissue (unpaired *t* test). Data in the scatter plots are presented as mean ± SD. Dots represent expression values from different tips from all biological replicates. a.u. = arbitrary units; %Lmair = linear intercept of air space; ns = not significant; pcw = postconception weeks; %Vair = volume densities of air space.

Downloaded from academic.oup.com/ajrccm/article/211/6/992/8513773 by Universidad de Desarrollo user on 16 November 2026

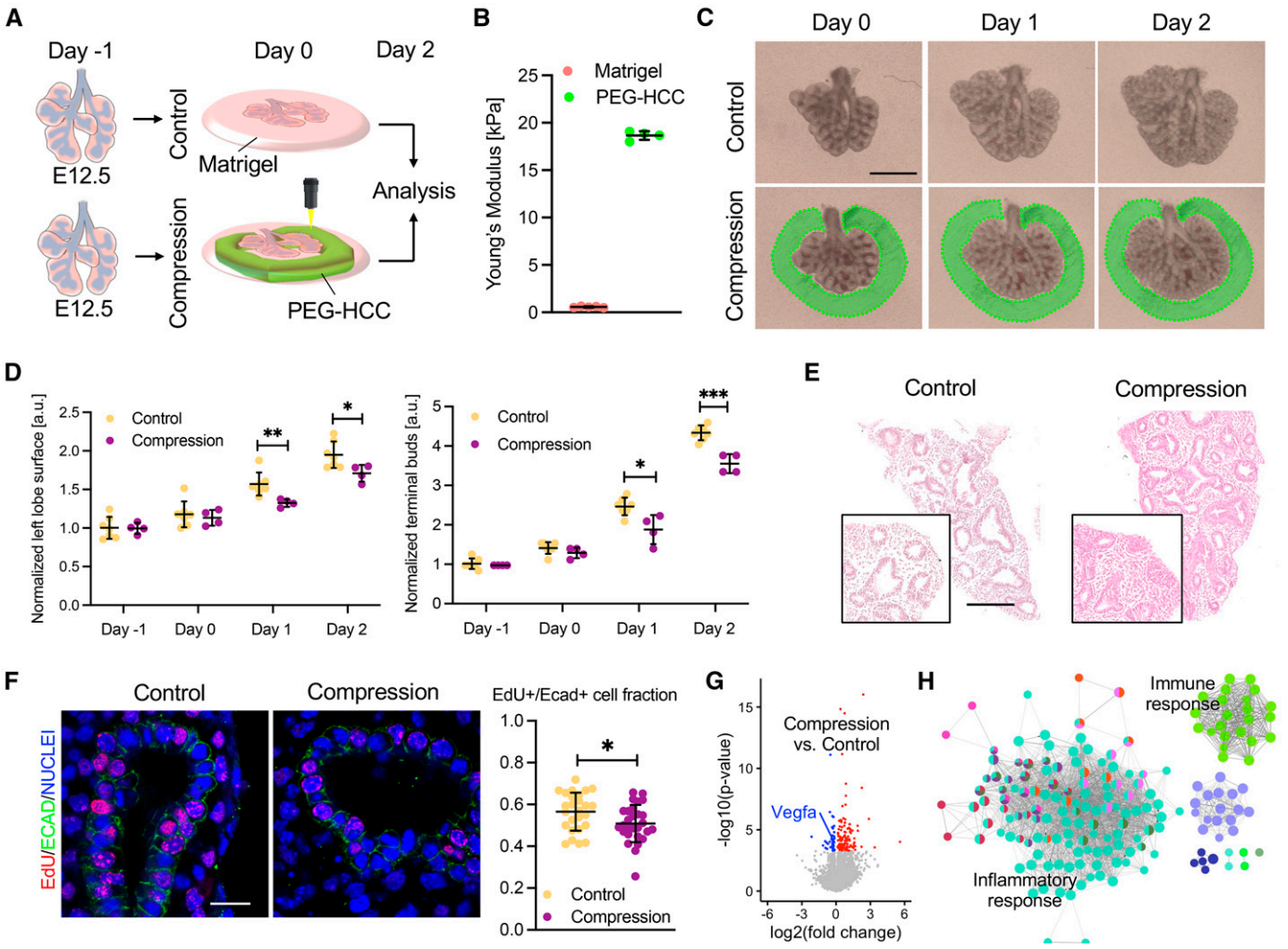


Figure 2. (*A*) Experimental setup of the *ex vivo* model of mouse fetal lung compression during pseudoglandular stage. Freshly isolated mouse fetal lungs (gestational day 12.5) were embedded in Matrigel drops and cultured in air–liquid interface. The next day (Day 0), a 20% coumarin HCC-conjugated eight-arm polyethylene glycol gel solution was dispersed into the Matrigel drop and selectively cross-linked under a two-photon microscope to surround the lungs and inhibit their growth over a total of 2 days. Control lungs had the same amount of polyethylene glycol gel solution added to the Matrigel, but this was not cross-linked with the two-photon laser. (*B*) Atomic force microscopy analysis confirms that the stiffness of the gel in culture conditions after 2 weeks from printing is approximately 20-fold higher compared with Matrigel. (*C*) Representative time-lapse imaging of lung growth under physical confinement (compression) compared with control. Scale bars, 100 μm. (*D*) Quantification of left lobe surface area (left) and terminal buds (right) in control and compressed lungs after 2 days of mechanical confinement for the following biological replicates: control ($n = 6$) and compression ($n = 4$). Mann-Whitney test: $^{*}P < 0.05$, $^{**}P < 0.01$, and $^{***}P < 0.001$. Data are presented as mean ± SD. Dots represent biological replicates. (*E*) Representative hematoxylin and eosin staining of control ($n = 2$) and compressed ($n = 2$) lungs after 2 days of mechanical confinement. Scale bars, 100 μm. (*F*) EdU (5-ethynyl-2-deoxyuridine) incorporation assay after 2 days of mechanical confinement for the following biological replicates: control ($n = 3$) and compression ($n = 3$) (unpaired *t* test, $^{*}P < 0.05$). Data are presented as mean ± SD. Dots represent single-tip quantification from all biological replicates. (*G*) Volcano plot of bulk RNA sequencing analysis of compressed versus control lungs after 2 days of mechanical confinement. Differentially expressed genes have been identified with fold change >1.1 and $P < 0.05$. Differentially expressed gene analysis shows downregulation of *Vegfa* in compressed lungs. (*H*) Gene network analysis of overexpressed genes in the compressed lungs reveals upregulation of categories related to inflammatory and immune response. Ecad = E-cadherin; PEG-HCC = coumarin HCC-conjugated eight-arm polyethylene glycol gel.

salutary effect was reversed by the KDR/Flk1 inhibitor SU5416 (45, 46) (Figures 3K and 3L). Overall, these data suggest that VEGF could restore epithelial proliferation in the distal lung when this is exposed to mechanical confinement.

Exogenous VEGF Supplementation Promotes Lung Growth and Ameliorates Airway Abnormalities in the Nitrofen Rat Model of CDH

To test the therapeutic value of VEGF *in vivo*, we sought to determine whether VEGF supplementation would be salutary (beyond TO) against pulmonary hypoplasia in the nitrofen rat model of CDH. We developed an ND VEGF delivery platform (ND-VEGF) to allow spatially and temporally targeted release of VEGF in fetal

Downloaded from academic.oup.com/ajrcmb/article/211/6/992/8513773 by Universidad de Desarrollo user on 16 November 2026

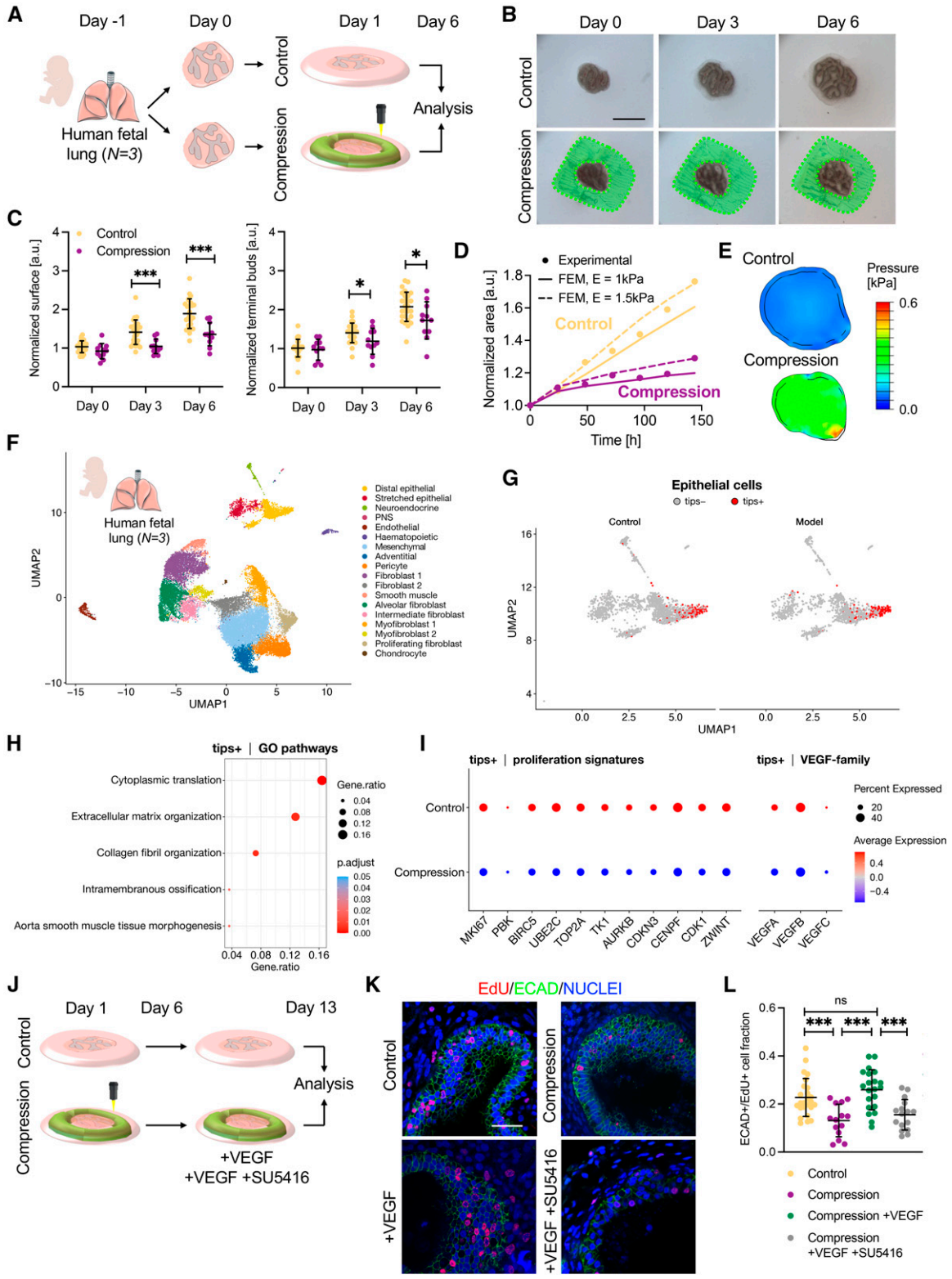


Figure 3. (*A*) Experimental setup of the *ex vivo* model of human fetal lung compression during the pseudoglandular stage. (*B*) Representative time-lapse imaging of human lung tissue growth under physical confinement (compression) compared with control ($n = 4$ biological replicates; scale bars, 100 μm). (*C*) Quantification of human lung tissue surface area (left) and terminal buds (right) in control and compressed lungs after 6 days of mechanical confinement for the following biological replicates: control ($n = 3$) and compression ($n = 3$). Mann-Whitney test, $^{*}P < 0.05$, and $^{***}P < 0.001$. Data in the scatter plots are presented as mean ± SD. Dots represent different technical replicates from all

Downloaded from academic.oup.com/ajrccm/article/211/6/992/8513773 by Universidad de Desarrollo user on 16 November 2026

lungs *in vivo* (25 ng/g fetal weight). The effect of ND-VEGF was compared with that of TO alone as well as free VEGF in solution and coadministered SU5416 to confirm VEGF specificity (Figure 4A). Ultrasound assessment at E19 was 100% accurate in detecting fetuses with CDH as confirmed at harvesting (E21; Figure 4B), and only these were included in the study (CDH incidence, 40%). Fetuses with leakage during intratracheal administration were excluded ($n = 6$). A total of 168 CDH fetuses from 54 time-dated pregnant rats were included. There was no difference in fetal survival between groups (Figure E8). ND-VEGF was identified only within the distal airways of CDH rats at E21, with evidence of retention of VEGF by E-cadherin–positive epithelial cells (Figure 4C) and no leakage to other fetal or maternal tissues. Histopathological analysis of fetal and maternal tissues demonstrated no toxic effects of empty ND, free VEGF, or ND-conjugated VEGF. In addition to the lack of pulmonary edema, free and ND-conjugated VEGF did not result in microscopic abnormalities or neovascular growth in the placenta, fetal, or maternal organs (Figures E9 and E10). Moreover, there was no effect of ND-VEGF on fetal and maternal hematological and biochemical parameters (Figure E11).

Lungs in the sham group were the smallest macroscopically, those in the ND-VEGF + TO group were the largest, and the lungs in other groups were in between (Figure 5A). Lung–to–body weight ratio (LBWR) and total lung protein content in untreated CDH fetuses were markedly reduced compared with healthy controls ($P < 0.0001$; Figures 5B and 5C). TO resulted in a significant increase in LBWR ($P < 0.0001$) and protein content ($P < 0.0001$) compared with sham (Figures 5B and 5C). ND-VEGF followed by TO had effects that were complementary to those of TO alone ($P < 0.0001$ vs. sham and PBS + TO) and normalized lung size (Figures 5B and 5C). This effect was not observed when free VEGF or empty ND were administered, and was abrogated by coadministration of SU5416 ($P < 0.0001$ vs. ND-VEGF + TO; Figures 5B and 5C). As described previously, nitrofen-induced CDH resulted in marked abnormalities in airway morphology (mean linear intercept of wall transection length [Lmw], mean linear intercept of parenchymal airspace [Lma], mean terminal bronchiolar density; $P < 0.0001$ vs. healthy; Figures 5D, 5E, and E12). TO resulted in partial improvement in these parameters ($P < 0.05$ vs. sham; Figures 5D, 5E, and E12). ND-VEGF had salutary effects on lung morphology beyond those achieved by TO alone and normalized distal airway maturation in CDH animals (Lmw/Lma, $P < 0.0001$ vs. sham and $P < 0.05$ vs. PBS + TO; Figure 5E), but there was no normalization of the number of alveolar saccules (*see* Figure E12). The therapeutic benefit of ND-VEGF was not observed when free VEGF (Lmw/Lma, $P < 0.01$ vs. ND-VEGF + TO) or empty ND (Lmw/Lma, $P < 0.001$ vs. ND-VEGF + TO) were administered and was abrogated by coadministration of SU5416 (Lmw/Lma, $P < 0.001$ vs. ND-VEGF + TO; Figure 5E). SPC expression in ND-VEGF + TO animals was similar to healthy controls and significantly higher than in sham-treated animals ($P < 0.0001$; Figures 5F and 5G). SU5416 coadministration inhibited ND-VEGF–induced alveolar epithelial cell maturation ($P < 0.0001$; Figure 5G), and TO alone (or in conjunction with free VEGF or empty ND) did not affect SPC expression (Figures 5F and 5G).

Exogenous VEGF Supplementation Ameliorates Pulmonary Vascular Abnormalities in the Nitrofen Rat Model of CDH

Nitrofen-induced CDH was associated with increased muscularization of peripheral pulmonary arterioles (diameter, 30–50 μm) as well as reduced overall alveolar vascularization (Figures 5H and 5J). MT in the sham group was higher ($P < 0.0001$; Figures 5H and 5I), and thrombomodulin expression (thrombomodulin$^+$ immunohistochemistry index, a surrogate marker of pulmonary vascularization) in alveolar tissue was lower ($P < 0.0001$; Figures 5J and 5K) compared with healthy controls. TO alone attenuated pulmonary arteriolar muscularization to levels that were still significantly higher than in healthy controls ($P < 0.01$; Figure 5I) but had no effect on alveolar vascularization (Figure 5K). ND-VEGF in conjunction with TO was the only intervention that resulted in near-normalization of arterial muscularization ($P < 0.001$ vs. PBS + TO; Figures 5H and 5I) and overall alveolar vascularization ($P < 0.001$ vs. PBS + TO; Figures 5J and 5K), but these effects were reversed when SU5416 was coadministered (MT/thrombomodulin$^+$ immunohistochemistry index, $P < 0.001$ vs. ND-VEGF + TO; Figures 5K and 5I). Pulmonary arteriolar adventitial thickness

Figure 3. (*Continued*). biological replicates. (*D*) Finite element method (FEM) analysis validation based on the time-course experiment in Figure E2E. Comparison of normalized area of the lung sample over time for experimental data and numerical values from FEM analysis. FEM analysis was developed by adopting two values of the Young's modulus to account for the uncertainty about the stiffness of the human lung tissue. (*E*) Pressure field prediction. Representative pressure field (in kPa) for control and compressed lung fragments at Day 6, assuming a Young's modulus of 1.5 kPa for the human lung tissue. (*F*) Uniform Manifold Approximation and Projection (UMAP) visualization of 32,630 fetal lung cells from three biological replicates. Leiden clustering revealed 18 distinct cell types within mesenchymal, epithelial, endothelial, and hematopoietic fractions. (*G*) Magnified UMAP plot of the epithelial compartment cells. Distal tip cells (tips$^+$) were identified by coexpression of known tip markers (*SOX9*$^+$, *TESC*$^+$); the remaining cells comprise non-tip epithelium (tips$^-$). (*H*) GO enrichment analysis reveals differential expression of several gene profiles in tips$^+$ cells of the congenital diaphragmatic hernia model. (*I*) Relative expression of 11 proliferation-associated genes and 3 VEGF-family genes between control and congenital diaphragmatic hernia model tips. (*J*) Experimental setup of the human *ex vivo* model to test exogenous VEGF supplementation. After 7 days of culture in basal medium, compressed human lung fragments were treated with recombinant VEGF for an additional 7 days using the specific KDR/Flk1 (VEGF receptor 2) inhibitor SU5416 as a negative control. (*K*) Representative pictures of EdU (5-ethynyl-2-deoxyuridine) proliferation assay after 7 days of VEGF treatment (compression + VEGF) compared with control, compression only, and compressed samples treated with the VEGF-specific inhibitor SU5416. Immunostaining for E-cadherin was used to identify epithelial cells. Scale bars, 100 μm. (*L*) Quantification of the number of E-cadherin/EdU double-positive cells after 7 days of VEGF treatment for the following biological replicates: control ($n = 2$) and compression ($n = 2$) (unpaired *t* test, ***$P < 0.001$). Data are presented as mean ± SD. Dots represent values from different epithelial tips from different technical replicates of the same biological replicate. ECAD = E-cadherin; GO = Gene Ontology; ns = not significant.

Downloaded from academic.oup.com/ajrcm/article/211/6/992/8513773 by Universidad de Desarrollo user on 16 November 2026

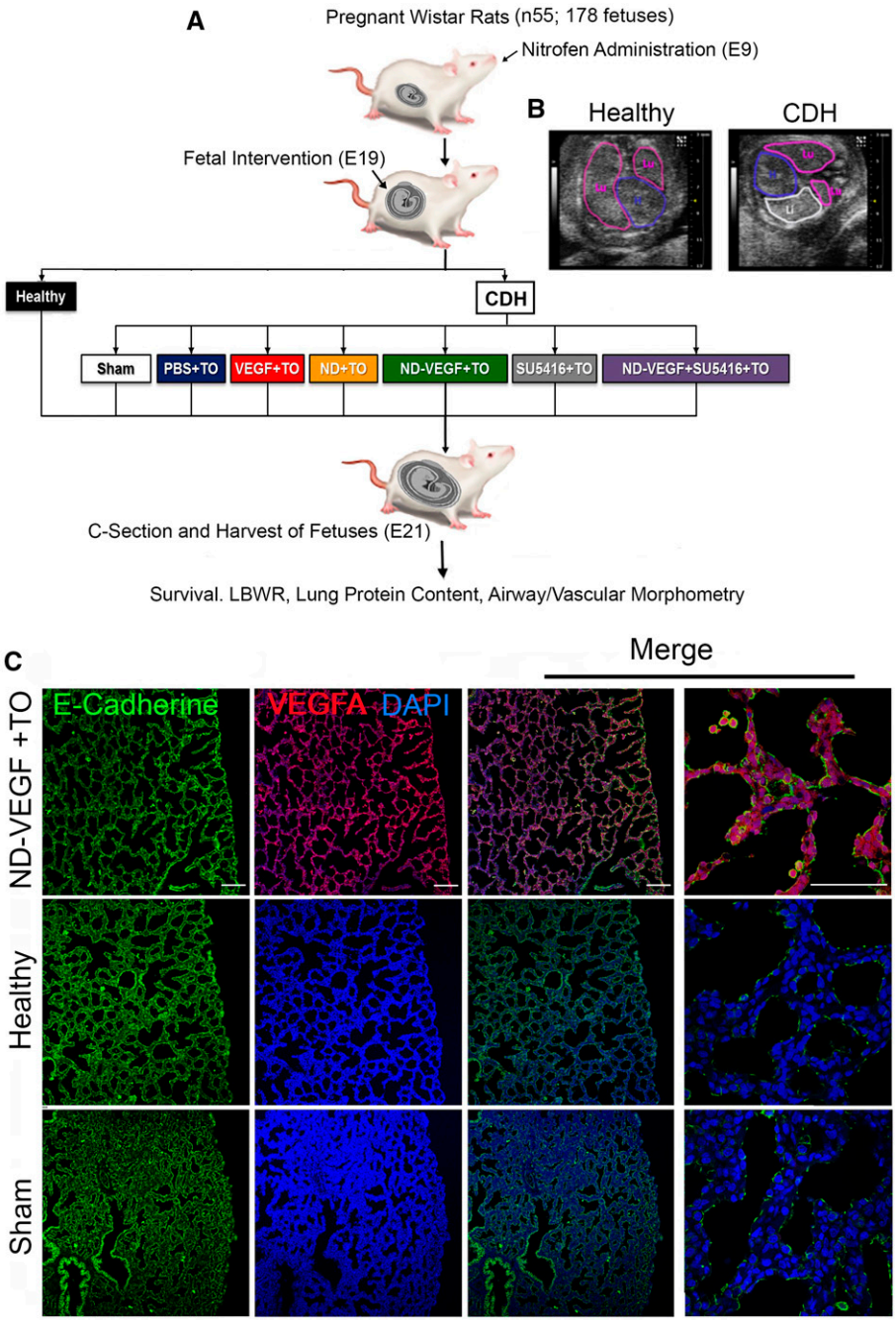


Figure 4. (*A*) Experimental design of *in vivo* intervention studies in fetal rats using VEGF-loaded nanodiamonds (ND-VEGF). There were eight experimental groups: healthy control (non–congenital diaphragmatic hernia [CDH], olive oil gavage-fed mothers; $n = 10$), sham intervention (surgery but no injection or tracheal occlusion [TO] in CDH fetuses from nitrofen-fed mothers; $n = 18$ underwent sham surgery), PBS + TO (intratracheal vehicle injection at gestational day 19 [E19] followed by TO in CDH fetuses; $n = 17$ underwent PBS solution injection followed by TO), free VEGF + TO (free VEGF injection followed by TO; $n = 40$), ND + TO (unconjugated ND-NH_2 injection followed by TO; $n = 35$), ND-VEGF + TO (ND-VEGF injection followed by TO; $n = 34$), SU5416 + TO (KDR/Flk1 inhibitor SU5416 injection followed by TO; $n = 11$), and ND-VEGF+SU5416 + TO (ND-VEGF and SU5416 coinjection followed by TO; $n = 13$). Animals in the groups with ND-VEGF administration received 13.4 ± 1.9 μg ND and 100 ng VEGF, whereas animals in the ND + TO and VEGF + TO groups received the same amounts of ND-NH_2 and free thiolated VEGF in 50 μl of PBS solution. The concentration of the KDR/Flk1 inhibitor SU5416 in the injection solution used in SU5416 + TO and ND-VEGF + SU5416 + TO groups was 120 μg/ml. (*B*) Confirmation of the presence of diaphragmatic defect in E18 fetal rats using micro-ultrasound (pink outline, lung; purple outline, heart; white outline, liver). (*C*) Representative confocal microscopy image demonstrating localization of ND-VEGF in airways at gestational day 21 following gestational-day 19 intratracheal administration of TO, with evidence of uptake/retention of VEGF by E-cadherin–expressing alveolar epithelial cells (E-cadherin, green; VEGF, red; DAPI, blue; magnification columns 1–3, ×20; magnification column 4, ×63; scale bars, 100 μm). E = gestational day.

Downloaded from academic.oup.com/ajrccm/article/211/6/992/8513773 by Universidad de Desarrollo user on 16 November 2026

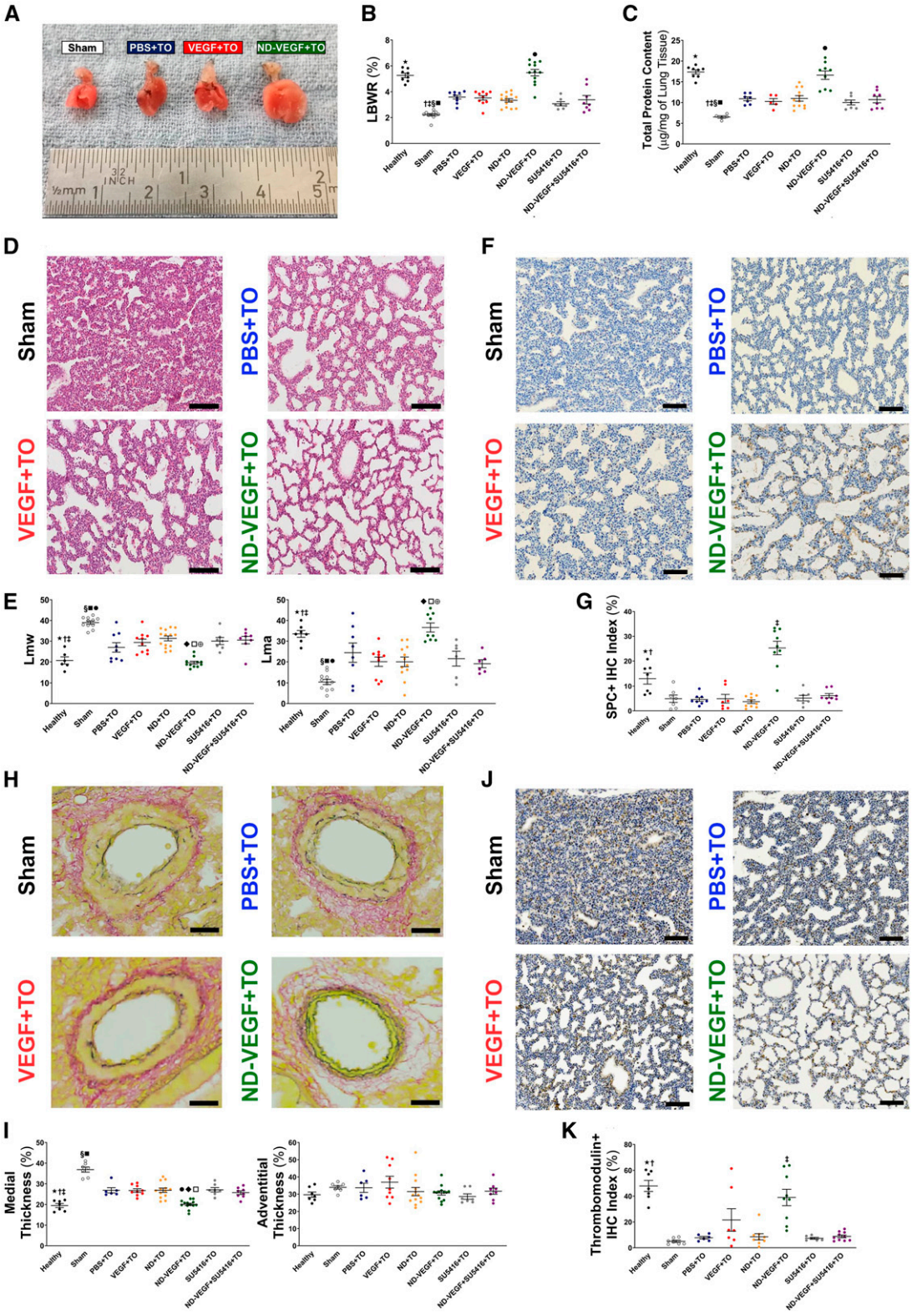


Figure 5. (*A*) Representative images of gestational day 21 (E21) lungs from rats in the intervention study (left to right: sham, PBS solution + tracheal occlusion [TO], VEGF + TO, nanodiamond (ND)-VEGF + TO). (*B*) Summary of lung–to–body weight ratio data (expressed as a percentage; $^{*}P < 0.0001$, healthy [$n = 8$] vs. sham [$n = 11$], PBS + TO [$n = 9$], ND + TO [$n = 14$], VEGF + TO [$n = 10$], SU5416 + TO [$n = 7$] and ND-VEGF + SU5416 + TO [$n = 8$]; $^{\dagger}P < 0.0001$ vs. PBS + TO and ND-VEGF + TO [$n = 12$]; $^{\ddagger}P < 0.001$ vs. ND + TO and VEGF + TO; $^{\S}P < 0.01$ vs. ND-VEGF + SU5416 + TO; ■$P < 0.05$ vs. SU5426 + TO; ●$P < 0.0001$ vs. PBS + TO, ND + TO, VEGF + TO, SU5426 + TO, and

Downloaded from academic.oup.com/ajrcm/article/211/6/992/8513773 by Universidad de Desarrollo user on 16 November 2026

was similar in all experimental groups (Figure 5I).

Toward Clinical Translation: Therapeutic Effects of VEGF Supplementation against Airway and Pulmonary Vascular Abnormalities in the Surgical Rabbit Model of CDH

We then tested the efficacy of our ND-VEGF platform in the rabbit model of CDH (Figure 6A). In this model, TO has been shown to ameliorate airway pathology but only to partly correct pulmonary vascular abnormalities (36). We therefore hypothesized that administration of ND-VEGF at the time of TO would have an additive effect to that of TO and normalize the pulmonary vasculature. A total of 50 fetuses from 20 time-dated pregnant rabbits underwent surgery for CDH creation at E23. At the time of fetal intervention (E28), the fetal survival rate was 44%. We tested ND-VEGF(low) by delivering a low dose of VEGF (25 ng/g of fetal weight, equivalent to that administered in the rat study), as well as ND-VEGF(high) (125 ng/g of fetal weight), in conjunction with TO. Fetuses with significant leakage during intratracheal administration were excluded ($n = 2$). Eighteen CDH fetuses and six healthy controls were included in subsequent analyses. Histopathological inspection of fetal and maternal tissues demonstrated no toxic effects of ND-VEGF (including pulmonary edema and acute lung injury scores; Figure E13) (47).

There was no difference in survival following fetal intervention between experimental groups (Figure 6B). LBWR in untreated CDH fetuses was reduced compared with controls ($P < 0.05$; Figure 6C). ND-VEGF(low) followed by TO led to a lung size comparable to controls ($P < 0.01$ vs. sham; Figure 6C), and a similar (albeit nonsignificant) trend was observed with ND-VEGF(high) (Figure 6C). In general, ND-VEGF in conjunction with TO resulted in normalization of airway morphometry abnormalities (Figures 6D, 6E, and E14), buy this was similar to what has been observed with TO alone (36). Interestingly, ND-VEGF(high) abrogated the beneficial effects of TO on Lma ($P < 0.05$; Figure 6E).

Vessel branching to the fifth order (i.e., peripheral branching) was significantly different between groups (Figures 6F and 6G). Administration of ND-VEGF(low) together with TO improved vascular branching to levels beyond what has been previously observed with TO alone (36), and similar to healthy controls ($P < 0.001$ vs. sham; Figure 6G). Unexpectedly, ND-VEGF(high) animals had a reduced number of peripheral vessels compared with controls and animals receiving ND-VEGF(low) ($P < 0.01$; Figures 6F and 6G). The main pulmonary artery acceleration/ejection time was reduced in CDH animals and, in contrast to what has been observed with TO alone (36), was normalized by ND-VEGF(low) and ND-VEGF(high) in conjunction with TO ($P < 0.05$; Figure 6H). No differences in right cardiac output or in the Doppler waveform of the right pulmonary artery branch was observed among groups. Vascular morphometric analysis in vessels <100 μm in diameter demonstrated a trend for increased MT in sham-operated animals that was not affected by coadministration of ND-VEGF(low) or

Figure 5. (*Continued*). ND-VEGF + SU5416 + TO; one-way ANOVA with Bonferroni *post hoc* tests). (*C*) Summary of total protein content data (expressed as μg/mg of lung tissue; ★$P < 0.0001$ healthy [$n = 8$] vs. sham [$n = 5$], PBS + TO [$n = 7$], ND + TO [$n = 12$], VEGF + TO [$n = 5$], SU5416 + TO [$n = 7$], and ND-VEGF + SU5416 + TO [$N = 8$]; †$P < 0.0001$ vs. PBS + TO and ND-VEGF + TO [$n = 9$]; ‡$P < 0.001$ vs. ND + TO and VEGF + TO; §$P < 0.01$ vs. ND-VEGF + SU5416 + TO; ■$P < 0.05$ vs. SU5426 + TO; ●$P < 0.0001$ vs. PBS + TO, ND + TO, VEGF + TO, SU5426 + TO, and ND-VEGF + SU5416 + TO; one-way ANOVA with Bonferroni *post hoc* tests). (*D*) Representative images of sections of E21 rat lungs from animals included in the *in vivo* intervention studies. Tissues were stained with hematoxylin and eosin and were used for subsequent airway morphometry analyses (magnification, ×20; scale bars, 100 μm). (*E*) Summary of mean linear intercept of wall transection length data (★$P < 0.0001$, healthy [$n = 6$] vs. sham [$n = 11$]; †$P < 0.01$ vs. VEGF + TO [$n = 10$], ND + TO [$n = 14$], SU5426 + TO [$n = 7$], and ND-VEGF + SU5426 + TO [$n = 8$]; ‡$P < 0.05$ vs. PBS + TO [$n = 9$]; §$P < 0.0001$ vs. ND-VEGF + TO [$n = 11$]; ■$P < 0.001$ vs. PBS + TO; ●$P < 0.01$ vs. VEGF + TO, ND + TO, SU5416 + TO, and ND-VEGF + SU5416 + TO; ◆$P < 0.001$ vs. ND + TO, SU5416 + TO, and ND-VEGF + SU5416 + TO; □$P < 0.01$ vs. VEGF + TO; ⊕$P < 0.05$ vs. PBS + TO; one-way ANOVA with Bonferroni *post hoc* tests) and mean linear intercept of parenchymal airspace data (★$P < 0.0001$, healthy [$n = 7$] vs. sham [$n = 11$]; †$P < 0.01$ vs. VEGF + TO [$n = 10$], ND + TO [$n = 12$], SU5426 + TO [$n = 6$], and ND-VEGF + SU5426 + TO [$n = 6$]; ‡$P < 0.05$ vs. PBS + TO [$n = 8$]; §$P < 0.0001$ vs. ND-VEGF + TO [$n = 9$]; ■$P < 0.001$ vs. PBS + TO; ●$P < 0.01$ vs. VEGF + TO, ND + TO, SU5416 + TO, and ND-VEGF + SU5416 + TO; ◆$P < 0.001$ vs. ND + TO, SU5416 + TO, and ND-VEGF + SU5416 + TO; □$P < 0.01$ vs. VEGF + TO; ⊕$P < 0.05$ vs. PBS + TO; one-way ANOVA with Bonferroni *post hoc* tests). (*F*) Representative images of lung sections from *in vivo* intervention studies stained for SPC (surfactant protein C; brown) using immunohistochemistry (IHC; magnification, ×20; scale bars, 100 μm). (*G*) Summary of SPC^+ IHC index (ratio of the number of SPC^+ cells over total cell number in predetermined areas of lung parenchyma; expressed as percentage) data (★$P < 0.0001$, healthy [$n = 7$] vs. sham [$n = 7$], PBS + TO [$n = 6$], ND + TO [$n = 9$], SU5416 + TO [$n = 6$], and ND-VEGF + SU5416 + TO [$n = 10$]; †$P < 0.01$ vs. VEGF + TO [$n = 7$]; ‡ND-VEGF + TO [$n = 9$]; $P < 0.0001$ vs. sham, PBS + TO, VEGF + TO, ND + TO, SU5416 + TO, and ND-VEGF + SU5416 + TO; one-way ANOVA with Bonferroni *post hoc* tests). (*H*) Representative images of sections of E21 rat lungs from animals included in the *in vivo* intervention studies. Miller's elastic staining was performed, and stained sections were used for subsequent vascular morphometry analyses (peripheral arterioles 30–50 μm in diameter; magnification, ×20; scale bars, 100 μm). (*I*) Summary of medial thickness data (expressed as a percentage of the external diameter of the blood vessel) (★$P < 0.0001$, healthy [$n = 7$] vs. sham [$n = 7$]; †$P < 0.01$ vs. VEGF + TO [$n = 7$], ND + TO [$n = 10$], SU5426 + TO [$n = 7$], and PBS + TO [$n = 8$]; ‡$P < 0.05$ vs. ND-VEGF + SU5426 + TO [$n = 8$]; §$P < 0.0001$ vs. ND-VEGF + TO [$n = 9$]; ■$P < 0.001$ vs. PBS + TO, VEGF + TO, ND + TO, SU5416 + TO, and ND-VEGF + SU5416 + TO; ●$P < 0.01$ vs. ND + TO; ◆$P < 0.001$ vs. PBS + TO and ND-VEGF + SU5416 + TO; □$P < 0.01$ vs. ND-VEGF + SU5426 + TO; one-way ANOVA with Bonferroni *post hoc* tests) and summary of adventitial thickness data (expressed as a percentage of the external diameter of the blood vessel). (*J*) Representative images of lung sections from *in vivo* intervention studies stained for thrombomodulin (brown) using IHC. (*K*) Summary of $thrombomodulin^+$ IHC index (ratio of the number of $thrombomodulin^+$ cells over total cell number in predetermined areas of lung parenchyma; expressed as percentage) data (★$P < 0.0001$, healthy [$n = 7$] vs. sham [$n = 7$], PBS + TO [$n = 6$], ND + TO [$n = 9$], SU5416 + TO [$n = 6$], and ND-VEGF + SU5416 + TO [$n = 10$]; †$P < 0.01$ vs. VEGF + TO [$n = 7$]; ‡$P < 0.001$ ND-VEGF + TO [$n = 9$] vs. sham, PBS + TO, ND + TO, SU5416 + TO, and ND-VEGF + SU5416 + TO; one-way ANOVA with Bonferroni *post hoc* tests). Lma = linear intercept of air space; Lmw = linear intercept of wall transection length.

Downloaded from academic.oup.com/ajrccm/article/211/6/992/8513773 by Universidad de Desarrollo user on 16 November 2026

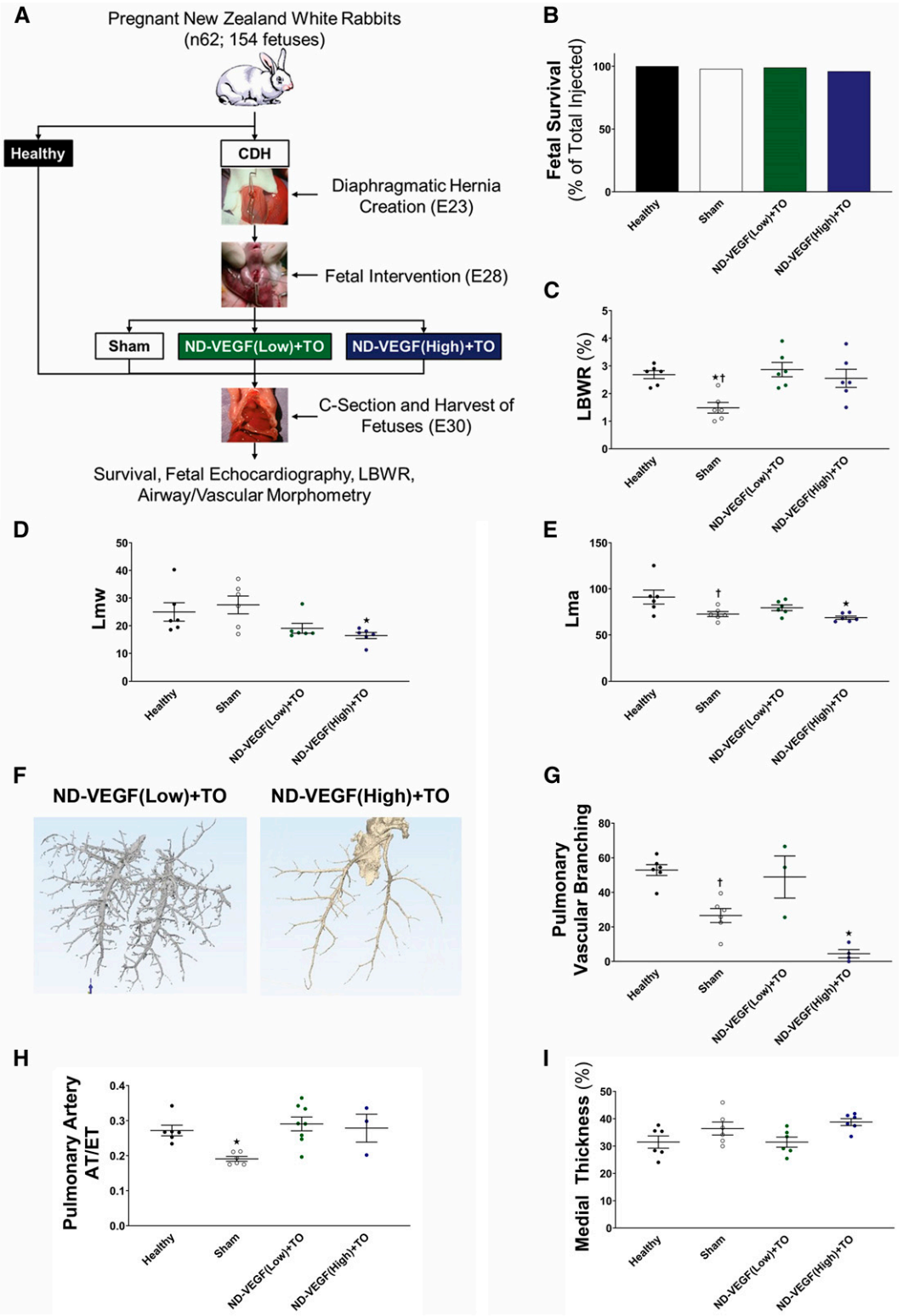


Figure 6. (*A*) Experimental design of *in vivo* intervention studies in fetal rabbits using VEGF-loaded nanodiamonds (ND-VEGF). There were four experimental groups: healthy control (non–congenital diaphragmatic hernia; $n = 6$), sham intervention (surgery but no injection or tracheal occlusion/tracheal occlusion [TO] in congenital diaphragmatic hernia fetuses; $n = 6$ underwent sham surgery), ND-VEGF(low) + TO (ND-VEGF with low-dose VEGF injection followed by TO; $n = 6$ underwent intratracheal injection followed by TO), and ND-VEGF(high) + TO (ND-VEGF with high-dose VEGF injection followed by TO; $n = 7$). Animals in the groups with ND-VEGF(low) administration received 375 ± 16 μg ND and 1 μg

Downloaded from academic.oup.com/ajrccm/article/211/6/992/8513773 by Universidad de Desarrollo user on 16 November 2026

ND-VEGF(high) with TO (Figure 6I). There were no differences in acceleration time between groups.

Discussion

Here we demonstrate that exogenous VEGF supplementation coupled with TO can rescue lung hypoplasia and pulmonary vascular abnormalities in CDH. Because failure of diaphragm closure starts manifesting at approximately 6 weeks after conception (9), we collected postmortem CDH tissue at the earliest possible gestation and confirmed impaired distal pulmonary VEGF expression. We also found impaired branching morphogenesis, along with reduced epithelial proliferation. We developed an *ex vivo* model using human fetal lung tissue and confirmed that mechanical compression alone is sufficient to induce morphological and transcriptional evidence of lung hypoplasia. In contrast to previous studies using lung organoids to model CDH (48), we propose a whole fetal lung tissue compression model including all cell types present at a stage at which CDH likely starts manifesting *in vivo*. A preliminary characterization of the model using embryonic mouse lung showed impaired branching morphogenesis and reduced epithelial proliferation, similar to human CDH tissue. In addition, we found an overall transcriptional upregulation of inflammatory and immune response genes, along with a small but significant downregulation of *Vegfa*. Interestingly, an inflammatory response has been detected in the nitrofen model (39) and in human cord blood from CDH fetuses (49). We developed an FEM-based analysis to confirm that distal areas are stiffened compared with control. Using our model, we demonstrated for the first time in human fetal lung that mechanical compression alone decreases proliferation in bud tip progenitors. scRNA-seq revealed a reduced expression of *VEGF* in compressed epithelial bud tip progenitors, reflecting the significant VEGF impairment found later in CDH lungs. Although the mechanism through which mechanical alterations lead to VEGF impairment is unknown, we speculate that an autocrine/paracrine VEGF signaling that has been previously described in epithelial development and in different types of cancer (50–52) could be involved.

There is currently no *in vivo* evidence for a therapeutic effect of VEGF administration in CDH. Such administration would require tight temporal and spatial control to emulate normal development. NDs integrate several properties that make them suitable in this setting, including innate biocompatibility, scalability, and an easily adaptable carbon surface for bioagent attachment (53). Their use as a drug-delivery platform is effective in the preclinical treatment of chemotherapy-resistant tumors as a result of prolonged and sustained drug delivery (26).

We tested a therapeutic formulation whereby VEGF was coupled to ND structures. Chemical modification of the VEGF protein did not affect its biological activity (54). In our innovative system, VEGF covalently bound to NDs allowed sustained release. As expected, fluorescently labeled nanoparticles showed a nonuniform distribution with a granular aspect in the cytoplasm of pulmonary epithelial cells suggesting cellular uptake by endocytosis (55). The containment of the nanoparticles within endosomes prevents ejection by the cells' efflux pump mechanism, but also inhibits penetration deep into the cytosol; this is an advantage because VEGF functions primarily extracellularly in fetal airway development (56). Importantly, even epithelial cells exposed to increasing concentrations of ND for prolonged periods showed no changes in metabolic activity, proliferation, or apoptosis.

We then investigated the biological effects of VEGF in the nitrofen rat model (57). Pulmonary VEGF expression is reduced in CDH (11) but upregulated after TO, corresponding to substantial lung growth (34). We confirmed this and further demonstrated that the addition of injected substances did not increase mortality. Injection of unmodified VEGF did not further supplement the effect of TO, but injection of ND-VEGF normalized lung size and airway morphology. This effect was abolished when a VEGF inhibitor (45, 46) was injected alongside ND-VEGF. Moreover, gradual release of VEGF by ND-VEGF affected the lung vasculature with normalization of overall pulmonary parenchymal vascularization (assessed by expression of the endothelial marker thrombomodulin) (58), as well as MT of peripheral pulmonary arteries. TO alone only partially reversed these changes, and the effect disappeared when a VEGF inhibitor was added, confirming a VEGF-specific effect. We believe these findings also have relevance beyond CDH treatment, and our nanocarrier approach could be beneficial in other perinatal lung diseases in which VEGF plays a key role (21, 59). We confirmed the beneficial effects and translational relevance of the ND-VEGF platform in the surgical rabbit model of CDH.

There are several limitations to the present study. First, the mechanism of action is unclear, and, while specific, it is uncertain whether VEGF acts on endothelial cells only

Figure 6. (*Continued*). VEGF, whereas animals in the ND-VEGF(high) group received 375 ± 27 μg ND and 5 μg VEGF. (*B*) Summary of fetal survival data. (*C*) Summary of lung–to–body weight ratio data (expressed as a percentage) (★$P < 0.05$, sham [$n = 6$] vs. healthy [$n = 6$]; †$P < 0.01$ vs. ND-VEGF[low] + TO [$n = 6$]; one-way ANOVA with Bonferroni *post hoc* tests; $n = 6$ for the ND-VEGF[high] group). (*D*) Summary of mean linear intercept of wall transection length data (★$P < 0.05$, ND-VEGF[high] + TO [$n = 6$] vs. sham [$n = 6$]; one-way ANOVA with Bonferroni *post hoc* tests; $n = 6$ for the ND-VEGF[low] group). (*E*) Summary of mean linear intercept of parenchymal airspace data (★$P < 0.01$, ND-VEGF[high] + TO [$n = 6$] vs. healthy [$n = 6$] and ND-VEGF[low] + TO [$n = 6$]; †$P < 0.05$, sham [$n = 6$] vs. healthy and ND-VEGF[low] + TO; one-way ANOVA with Bonferroni *post hoc* tests). (*F*) Representative micro–computed tomography images (three-dimensionally reconstructed) of the pulmonary vasculature of fetal rabbits in the ND-VEGF(low) + TO and ND-VEGF(high) + TO groups. Such images were used for assessment of pulmonary vascular branching. (*G*) Summary of pulmonary vascular branching (at least fifth order; peripheral) data (expressed as percentage of total; ★$P < 0.001$, ND-VEGF[high] + TO [$n = 4$] vs. healthy [$n = 6$] and ND-VEGF[low] + TO [$n = 3$]; †$P < 0.01$, sham [$n = 6$] vs. healthy and ND-VEGF[low] + TO; one-way ANOVA with Bonferroni *post hoc* tests). (*H*) Summary of pulmonary artery acceleration/ejection time data obtained by pulmonary echocardiography (★$P < 0.05$, sham [$n = 6$] vs. healthy [$n = 6$], ND-VEGF[low] + TO [$n = 8$] and ND-VEGF[high] + TO [$n = 3$]; one-way ANOVA with Bonferroni *post hoc* tests). (*I*) Summary of medial thickness data (expressed as a percentage of the external diameter of the blood vessel; $n = 6$ for all experimental groups). AT/ET = acceleration time/ejection time; E = gestational day; LBWR = lung–to–body weight ratio; Lma = linear intercept of air space; Lmw = linear intercept of wall transection length.

Downloaded from academic.oup.com/ajrccm/article/211/6/992/8513773 by Universidad de Desarrollo user on 16 November 2026

or on pulmonary epithelial and endothelial cells. Furthermore, we did not assess the specificity and efficiency of nanoparticle uptake by various cell types in the fetal lung in our biodistribution study, and we did not formally measure VEGF nanoparticle "leakage" to other organs. However, we did not find any evidence of the human VEGF that was carried by ND-VEGF in any fetal or maternal tissues other than the fetal lung by immunofluorescence. Pulmonary tropism of our platform could be enhanced by modifying the carrier to bind to cell membranes of organ-specific cells (60). Another limitation of our study is that the ND core of our platform is not biodegradable, and long-term clearance studies would need to be performed before clinical translation. An alternative would be to replace the ND core with another biocompatible and biodegradable nanocarrier. Finally, local lung toxicity remains unclear *in vivo*; however, it was not significant in our studies, as previously reported (61). However, this should be further investigated because nanoparticles are taken up by local immune cells that may play critical roles in the induction and regulation of pulmonary immunity and inflammation (55).

In conclusion, we have demonstrated the role of VEGF in the maturation of human lung epithelium and its impairment in CDH. *In vitro* and *in vivo* data show that sustained VEGF stimulation rescued the affected lungs. Delivery of growth factors such as VEGF by NDs and other nanocarriers could have a place in perinatal lung therapy, with potential scalability for clinical use, and this will need to be further validated and optimized in preclinical models of CDH and TO before translation. ■

Author disclosures are available with the text of this article at www.atsjournals.org.

Downloaded from academic.oup.com/ajrccm/article/211/6/992/8513773 by Universidad de Desarrollo user on 16 November 2026

References

1. ScienceDirect. Lung hypoplasia—an overview | ScienceDirect Topics [accessed 2025 Feb 27]. Available from: https://www.sciencedirect.com/topics/nursing-and-health-professions/lung-hypoplasia.
2. Langham MR, Kays DW, Ledbetter DJ, Frentzen B, Sanford LL, Richards DS, *et al.* Congenital diaphragmatic hernia: epidemiology and outcome. *Clin Perinatol* 1996;23:671–688.
3. Kitagawa M, Hislop A, Boyden EA, Reid L. Lung hypoplasia in congenital diaphragmatic hernia. A quantitative study of airway, artery, and alveolar development. *Br J Surg* 1971;58:342–346.
4. Deprest J, De Coppi P. Antenatal management of isolated congenital diaphragmatic hernia today and tomorrow: ongoing collaborative research and development. *J Pediatr Surg* 2012;47:282–290.
5. DiFiore JW, Fauza DO, Slavin R, Peters CA, Fackler JC, Wilson JM, *et al.* Experimental fetal tracheal ligation reverses the structural and physiological effects of pulmonary hypoplasia in congenital diaphragmatic hernia. *J Pediatr Surg* 1994;29:248–257.
6. Khan PA, Cloutier M, Piedboeuf B. Tracheal occlusion: a review of obstructing fetal lungs to make them grow and mature. *Am J Med Genet C Semin Med Genet* 2007;145C:125–138.
7. Dekoninck P, Gratacos E, Van Mieghem T, Richter J, Lewi P, Ancel AM, *et al.* Results of fetal endoscopic tracheal occlusion for congenital diaphragmatic hernia and the set up of the randomized controlled TOTAL trial. *Early Hum Dev* 2011;87:619–624.
8. Flageole H, Evrard VA, Piedboeuf B, Laberge JM, Lerut TE, Deprest JA, *et al.* The plug-unplug sequence: an important step to achieve type II pneumocyte maturation in the fetal lamb model. *J Pediatr Surg* 1998;33:299–303.
9. Zani A, Chung WK, Deprest J, Harting MT, Jancelewicz T, Kunisaki SM, *et al.* Congenital diaphragmatic hernia. *Nat Rev Dis Primers* 2022;8:37.
10. Antounians L, Catania VD, Montalva L, Liu BD, Hou H, Chan C, *et al.* Fetal lung underdevelopment is rescued by administration of amniotic fluid stem cell extracellular vesicles in rodents. *Sci Transl Med* 2021;13:eaax5941.
11. Okazaki T, Sharma HS, Aikawa M, Yamataka A, Nagai R, Miyano T, *et al.* Pulmonary expression of vascular endothelial growth factor and myosin isoforms in rats with congenital diaphragmatic hernia. *J Pediatr Surg* 1997;32:391–394.
12. Chang R, Andreoli S, Ng Y-S, Truong T, Smith SR, Wilson J, *et al.* VEGF expression is downregulated in nitrofen-induced congenital diaphragmatic hernia. *J Pediatr Surg* 2004;39:825–828.
13. Muehlethaler V, Kunig AM, Seedorf G, Balasubramaniam V, Abman SH. Impaired VEGF and nitric oxide signaling after nitrofen exposure in rat fetal lung explants. *Am J Physiol Lung Cell Mol Physiol* 2008;294:L110–L120.
14. Jakkula M, Le Cras TD, Gebb S, Hirth KP, Tuder RM, Voelkel NF, *et al.* Inhibition of angiogenesis decreases alveolarization in the developing rat lung. *Am J Physiol Lung Cell Mol Physiol* 2000;279:L600–L607.
15. Le Cras TD, Markham NE, Tuder RM, Voelkel NF, Abman SH. Treatment of newborn rats with a VEGF receptor inhibitor causes pulmonary hypertension and abnormal lung structure. *Am J Physiol Lung Cell Mol Physiol* 2002;283:L555–L562.
16. Grover TR, Parker TA, Abman SH. Vascular endothelial growth factor improves pulmonary vascular reactivity and structure in an experimental model of chronic pulmonary hypertension in fetal sheep. *Chest* 2005;128:614S.
17. Shinkai M, Shinkai T, Montedonico S, Puri P. Effect of VEGF on the branching morphogenesis of normal and nitrofen-induced hypoplastic fetal rat lung explants. *J Pediatr Surg* 2006;41:781–786.
18. Acker SN, Seedorf GJ, Abman SH, Nozik-Grayck E, Partrick DA, Gien J, *et al.* Pulmonary artery endothelial cell dysfunction and decreased populations of highly proliferative endothelial cells in experimental congenital diaphragmatic hernia. *Am J Physiol Lung Cell Mol Physiol* 2013;305:L943–L952.
19. Sbragia L, Oria M, Scorletti F, Romero Lopez MDM, Schmidt AF, Levy B, *et al.* A novel surgical toxicological-free model of diaphragmatic hernia in fetal rats. *Pediatr Res* 2022;92:118–124.
20. Compernolle V, Brusselmans K, Acker T, Hoet P, Tjwa M, Beck H, *et al.* Loss of HIF-2α and inhibition of VEGF impair fetal lung maturation, whereas treatment with VEGF prevents fatal respiratory distress in premature mice. *Nat Med* 2002;8:702–710.
21. Debeer A, Sbragia L, Vrancken K, Hendriks A, Roubliova X, Jani J, *et al.* Antenatal fetal VEGF therapy to promote pulmonary maturation in a preterm rabbit model. *Early Human Development* 2010;86:99–105.
22. George EM, Liu H, Robinson GG, Mahdi F, Perkins E, Bidwell GL, *et al.* Growth factor purification and delivery systems (PADS) for therapeutic angiogenesis. *Vasc Cell* 2015;7:1.
23. Peer D, Karp JM, Hong S, Farokhzad OC, Margalit R, Langer R, *et al.* Nanocarriers as an emerging platform for cancer therapy. *Nat Nanotechnol* 2007;2:751–760.
24. Smith DM, Simon JK, Baker JR Jr. Applications of nanotechnology for immunology. *Nat Rev Immunol* 2013;13:592–605.
25. Mochalin VN, Shenderova O, Ho D, Gogotsi Y. The properties and applications of nanodiamonds. *Nat Nanotechnol* 2011;7:11–23.
26. Chow EK, Zhang XQ, Chen M, Lam R, Robinson E, Huang H, *et al.* Nanodiamond therapeutic delivery agents mediate enhanced chemoresistant tumor treatment. *Sci Transl Med* 2011;3:73ra21.
27. Shibuya S, Allen-Hyttinen J, De Coppi P, Michielin F. In vitro models of fetal lung development to enhance research into congenital lung diseases. *Pediatr Surg Int* 2021;37:561–568.
28. Urciuolo A, Giobbe GG, Dong Y, Michielin F, Brandolino L, Magnussen M, *et al.* Hydrogel-in-hydrogel live bioprinting for guidance and control of organoids and organotypic cultures. *Nat Commun* 2023;14:3128.
29. Carlsson J, Drevin H, Axén R. Protein thiolation and reversible protein-protein conjugation. *N*-succinimidyl 3-(2-pyridyldithio)propionate, a new heterobifunctional reagent. *Biochem J* 1978;173:723–737.
30. Stan RV. Multiple PV1 dimers reside in the same stomatal or fenestral diaphragm. *Am J Physiol Heart Circ Physiol* 2004;286:H1347–H1353.

31. Mader C, Huber C, Moll D, Sleytr UB, Sára M. Interaction of the crystalline bacterial cell surface layer protein SbsB and the secondary cell wall polymer of geobacillus stearothermophilus PV72 assessed by real-time surface plasmon resonance biosensor technology. *J Bacteriol* 2004;186:1758–1768.
32. Kluth D, Kangah R, Reich P, Tenbrinck R, Tibboel D, Lambrecht W, *et al.* Nitrofen-induced diaphragmatic hernias in rats: an animal model. *J Pediatr Surg* 1990;25:850–854.
33. Wu J, Yamamoto H, Gratacos E, Ge X, Verbeken E, Sueishi K, *et al.* Lung development following diaphragmatic hernia in the fetal rabbit. *Hum Reprod* 2000;15:2483–2488.
34. Kanai M, Kitano Y, von Allmen D, Davies P, Adzick NS, Flake AW, *et al.* Fetal tracheal occlusion in the rat model of nitrofen-induced congenital diaphragmatic hernia: tracheal occlusion reverses the arterial structural abnormality. *J Pediatr Surg* 2001;36:839–845.
35. Kitano Y, Kanai M, Davies P, von Allmen D, Yang EY, Radu A, *et al.* BAPS Prize—1999: lung growth induced by prenatal tracheal occlusion and its modifying factors: a study in the rat model of congenital diaphragmatic hernia. *J Pediatr Surg* 2001;36:251–259.
36. Russo FM, Da Cunha MGMCM, Jimenez J, Lesage F, Eastwood MP, Toelen J, *et al.* Complementary effect of maternal sildenafil and fetal tracheal occlusion improves lung development in the rabbit model of congenital diaphragmatic hernia. *Ann Surg* 2022;275:e586–e595.
37. Lipsett J. Human fetal lung morphometry at autopsy with new modeling to quantitate structural maturity. *Pediatr Pulmonol* 2017;52:771–778.
38. Urciuolo A, Poli I, Brandolino L, Raffa P, Scattolini V, Laterza C, *et al.* Intravital three-dimensional bioprinting. *Nat Biomed Eng* 2020;4: 901–915.
39. Wagner R, Lieckfeldt P, Piyadasa H, Markel M, Riedel J, Stefanovici C, *et al.* Proteomic profiling of hypoplastic lungs suggests an underlying inflammatory response in the pathogenesis of abnormal lung development in congenital diaphragmatic hernia. *Ann Surg* 2023;278: e411–e421.
40. Dylong F, Riedel J, Amonkar GM, Peukert N, Lieckfeldt P, Sturm K, *et al.* Overactivated epithelial NF-κB disrupts lung development in congenital diaphragmatic hernia. *Am J Respir Cell Mol Biol* 2023;69:545–555.
41. He P, Lim K, Sun D, Pett JP, Jeng Q, Polanski K, *et al.* A human fetal lung cell atlas uncovers proximal-distal gradients of differentiation and key regulators of epithelial fates. *Cell* 2022;185:4841–4860.e25.
42. Nguyen TM, van der Merwe J, Elowsson Rendin L, Larsson-Callerfelt AK, Deprest J, Westergren-Thorsson G, *et al.* Stretch increases alveolar type 1 cell number in fetal lungs through ROCK-Yap/Taz pathway. *Am J Physiol Lung Cell Mol Physiol* 2021;321:L814–L826.
43. Copland IB, Post M. Stretch-activated signaling pathways responsible for early response gene expression in fetal lung epithelial cells. *J Cell Physiol* 2007;210:133–143.
44. Travaglini KJ, Nabhan AN, Penland L, Sinha R, Gillich A, Sit RV, *et al.* A molecular cell atlas of the human lung from single-cell RNA sequencing. *Nature* 2020;587:619–625.
45. Taraseviciene-Stewart L, Kasahara Y, Alger L, Hirth P, Mc Mahon G, Waltenberger J, *et al.* Inhibition of the VEGF receptor 2 combined with chronic hypoxia causes cell death-dependent pulmonary endothelial cell proliferation and severe pulmonary hypertension. *FASEB J* 2001; 15:427–438.
46. Oka M, Homma N, Taraseviciene-Stewart L, Morris KG, Kraskauskas D, Burns N, *et al.* Rho kinase–mediated vasoconstriction is important in severe occlusive pulmonary arterial hypertension in rats. *Circ Res* 2007;100:923–929.
47. Matute-Bello G, Downey G, Moore BB, Groshong SD, Matthay MA, Slutsky AS, *et al.*; Acute Lung Injury in Animals Study Group. An official American Thoracic Society Workshop Report: features and measurements of experimental acute lung injury in animals. *Am J Respir Cell Mol Biol* 2011;44:725–738.
48. Kunisaki SM, Jiang G, Biancotti JC, Ho KKY, Dye BR, Liu AP, *et al.* Human induced pluripotent stem cell-derived lung organoids in an ex vivo model of the congenital diaphragmatic hernia fetal lung. *Stem Cells Transl Med* 2021;10:98–114.
49. Fleck S, Bautista G, Keating SM, Lee TH, Keller RL, Moon-Grady AJ, *et al.* Fetal production of growth factors and inflammatory mediators predicts pulmonary hypertension in congenital diaphragmatic hernia. *Pediatr Res* 2013;74:290–298.
50. Lichtenberger BM, Tan PK, Niederleithner H, Ferrara N, Petzelbauer P, Sibilia M, *et al.* Autocrine VEGF signaling synergizes with EGFR in tumor cells to promote epithelial cancer development. *Cell* 2010;140: 268–279.
51. Peng S, Wang Y, Peng H, Chen D, Shen S, Peng B, *et al.* Autocrine vascular endothelial growth factor signaling promotes cell proliferation and modulates sorafenib treatment efficacy in hepatocellular carcinoma. *Hepatology* 2014;60:1264–1277.
52. Chatterjee S, Heukamp LC, Siobal M, Schöttle J, Wieczorek C, Peifer M, *et al.* Tumor VEGF:VEGFR2 autocrine feed-forward loop triggers angiogenesis in lung cancer. *J Clin Invest* 2013;123:1732–1740.
53. Krüger A, Liang Y, Jarre G, Stegk J. Surface functionalisation of detonation diamond suitable for biological applications. *J Mater Chem* 2006;16:2322–2328.
54. Fishman JM, Lowdell MW, Urbani L, Ansari T, Burns AJ, Turmaine M, *et al.* Immunomodulatory effect of a decellularized skeletal muscle scaffold in a discordant xenotransplantation model. *Proc Natl Acad Sci U S A* 2013;110:14360–14365.
55. Nelson SM, Hajivassiliou CA, Haddock G, Cameron AD, Robertson L, Olver RE, *et al.* Rescue of the hypoplastic lung by prenatal cyclical strain. *Am J Respir Crit Care Med* 2005;171:1395–1402.
56. Akeson AL, Greenberg JM, Cameron JE, Thompson FY, Brooks SK, Wiginton D, *et al.* Temporal and spatial regulation of VEGF-A controls vascular patterning in the embryonic lung. *Dev Biol* 2003;264: 443–455.
57. Newton DL, Hansen HJ, Mikulski SM, Goldenberg DM, Rybak SM. Potent and specific antitumor effects of an anti-CD22–targeted cytotoxic ribonuclease: potential for the treatment of non-Hodgkin lymphoma. *Blood* 2001;97:528–535.
58. Loghmani H, Conway EM. Exploring traditional and nontraditional roles for thrombomodulin. *Blood* 2018;132:148–158.
59. Thébaud B, Abman SH, Dysplasia B. Bronchopulmonary dysplasia: where have all the vessels gone? Roles of angiogenic growth factors in chronic lung disease. *Am J Respir Crit Care Med* 2007;175: 978–985.
60. Press AT, Traeger A, Pietsch C, Mosig A, Wagner M, Clemens MG, *et al.* Cell type-specific delivery of short interfering RNAs by dye-functionalised theranostic nanoparticles. *Nat Commun* 2014;5:5565.
61. Carlon MS, Engels AC, Bosch B, Joyeux L, Mori da Cunha MGMC, Vidović D, *et al.* A novel translational model for fetoscopic intratracheal delivery of nanoparticles in piglets. *Prenat Diagn* 2016;36:926–934.

Downloaded from academic.oup.com/ajrccm/article/211/6/992/8513773 by Universidad de Desarrollo user on 16 November 2026